Materials Advances

ROYAL SOCIETY OF CHEMISTRY

PAPER

View Article Online
View Journal | View Issue



Cite this: *Mater. Adv.*, 2022, 3, 389

# Bio-based copolyesters involving 1,4:3,6-dianhydrohexitols and sebacic acid: 2,6-pyridinedicarboxylic acid as platforms for high gas barrier food packaging†

Xuelian Liu, [a] Laurent Lebrun, *[b] Nadège Follain [b] and Nicolas Desilles *[a]

Received 2nd September 2021,
Accepted 21st October 2021

DOI: 10.1039/d1ma00797a

rsc.li/materials-advances

Proposing renewable structures for food packaging applications is necessary for contributing to a low-carbon and sustainable world. Thus, bio-based copolyesters, involving isosorbide (or isomannide), sebacoyl dichloride, and a second rigid acid structure (succinyl dichloride, isophthaloyl chloride or 2,6-pyridinedicarbonyl dichloride), were synthesized *via* polycondensation reactions. The $\overline{M_n}$ values ranged from 10 600 to 18 000 g mol$^{-1}$. $^1$H NMR spectroscopy established the random copolymerization and enabled the calculation of the respective monomer ratios in the copolymers. All copolyesters were thermally stable with $T_d^{5\%}$ higher than 328 °C and $T_g$ ranging from 30 to 64 °C. The tensile test revealed plastic fractures for aliphatic copolyesters and brittle fractures for aromatic ones. The highest Young's modulus and tensile strength were obtained for aromatic copolyesters, whereas the largest elongation at break was observed for aliphatic ones. All copolyesters showed good gas barrier properties, and the best result was comparable to the widely used semi-crystalline PET.

## 1. Introduction

In 2015, at the Paris Climate Conference (COP21), 196 parties came to an agreement to adopt the first-ever, legally binding global climate convention that decided to develop a low carbon society.[1] This convention came into force on 4th November 2016,[2] and a subsequent low-carbon world conference is planned by the France government to be conducted in June 2021 to further clarify national strategies.[3] Thus, our world is being highly promoted to move towards a low carbon society. To achieve this goal, a large number of research studies have been devoted to the development of clean energy and bio-based products. However, the current global food packaging market is still dominated by traditional polymeric materials, which conflicts the concept of low carbon and sustainable development. According to 2018 data, 45% of the global fossil fuel supplies not intended for energy purposes were used to produce plastics, which is expected to increase to 60% by 2050,[4] and the volume of food packaging plastics is estimated to be around 40% of the whole plastics consumption.[5] The extensive use of petroleum-based polymers is threatening our planet by depleting crude oil and accelerating global warming. Thus, more efforts are needed to develop polymers from bio-based feedstocks.

Among the various bio-based feedstocks, 1,4:3,6-dianhydrohexitols attracted much research attention in recent years. Besides, their molecular rigidity and chirality made them popular as platforms for developing new bio-based polymers with high glass transition temperature and/or special optical properties in the past decades.[6–8] Also, their non-toxicity allows them to be used in food packaging and bio-medical devices.[7,8] Particularly, the large scale production of high purity isosorbide (POLYSORB®) by Roquette further facilitates the development of low carbon footprint polymers based on this molecule such as polyesters, polycarbonates and thermoplastic polyurethanes (TPUs).[9,10] Furthermore, according to Okada *et al.*, the aliphatic polyesters based on 1,4:3,6-dianhydrohexitols are biodegradable, which further enhances their environmentally friendly competitiveness.[11]

Our previous work suggested that the aliphatic polyesters based on isosorbide (IS), or isomannide (IM), and sebacoyl chloride (C10), named ISC10 and IMC10, respectively, have the potential for food packaging application with satisfactory $CO_2$/$O_2$ selectivity ($\alpha_{CO_2/O_2}$).[12] However, their low glass transition temperature ($T_g$) might be a limitation in terms of mechanical, and water and gas barrier properties. Copolymerization with rigid (cyclic or aromatic) moieties and/or shorter aliphatic

[a] Normandie Université, INSA Rouen Normandie, CNRS UMR 6270, 685 Avenue de l'Université, 76800 Saint Etienne du Rouvray, France. E-mail: xuelian.liu@insa-rouen.fr, nicolas.desilles@insa-rouen.fr

[b] Normandie Université, Université Rouen Normandie, CNRS UMR 6270, Faculté des Sciences, 76821 Mont Saint Aignan, France. E-mail: laurent.lebrun@univ-rouen.fr, nadege.follain@univ-rouen.fr

† Electronic supplementary information (ESI) available: FTIR and $^1$H NMR spectra and some supplemental figures (DSC, tensile test), tables (TGA, gas permeation coefficients) and the tensile test video. See DOI: 10.1039/d1ma00797a

segments is usually considered as an effective strategy to obtain polyesters with enhanced $T_g$.[13] In addition, the properties can be readily tuned by varying the monomer type and the sequence of incorporation.[6] Succinic acid (SA) is one of the most popular short-chain aliphatic bio-based diacid, and its derivative succinyl dichloride (C4) has already shown potential for the preparation of high $T_g$ polyesters with IS or IM.[7,8] Besides, some rigid cyclic monomers, such as 2,5-furandicarboxylic acid (FDCA25) and vanillin, have also been used as bio-based cyclic building blocks.[14–16] Recently, another promising rigid structure containing a pyridine ring, named 2,6-pyridinedicarboxylic acid (PDA26) or dipicolinic acid, which could also be obtained from biomass, attracted our attention for the preparation of fully bio-based polyesters.[17,18]

PDA26 has a chemical structure similar to isophthalic acid (IPA), but its polar pyridine ring instead of a non-polar benzene ring may not only bring chain rigidity but also pyridine functionality.[17,18] As reported by Burgess *et al.*, poly(ethylene 2,5-furandicarboxylate) (PEF) showed 19 × $CO_2$, 11 × $O_2$ and 2 × $H_2O$ barrier compared to poly(ethylene terephthalate) (PET).[19] These excellent barrier properties of PEF compared to those of PET were attributed to its asymmetric polar furan ring.[19,20] The structural similarity and polarity of PDA26 to FDCA25 motivated us to investigate its influence on the properties of ISC10 and IMC10. Given the chelation of the pyridine ring with metal catalysts[18] and the spontaneous melting/decomposition (248–250 °C) of PDA26, the chlorine derivative, 2,6-pyridinedicarbonyl dichloride (PDD26), which is more active and has a much lower melting temperature ($T_m$ = 56–58 °C), was chosen as a better option for catalyst-free polymerization and evaluating the potential of the same structures as those that would be obtained with carboxylic acids from biomass.

Thus, this article will focus on the preparation of fully bio-based copolyesters, ISC10 and IMC10, by incorporating PDD26 or C4. For comparison, the copolyesters involving petroleum-based IPA will also be prepared. Comprehensive discussions on the thermal, mechanical and barrier properties will be done not only between aliphatic and aromatic structures, but also within aromatic structures (between polar pyridine and non-polar benzene rings).

# 2. Experimental section

## 2.1 Materials

Isosorbide (IS, 98%), isomannide (IM, 95%), succinyl chloride (C4, 95%), sebacoyl chloride (C10, ≥95%), 2,6-pyridinedicarbonyl dichloride (PDD26, 97%), ethylene glycol (>99%) and decane (>99%) were purchased from Sigma-Aldrich. Isophthaloyl chloride (IPC, 98%) was provided by Alfa Aesar. Dry toluene (99.85%) and dry pyridine (99.5%) were obtained from ACROS Organics. Dichloromethane ($CH_2Cl_2$, reagent grade) was purchased from Fisher Scientific. Methanol ($CH_3OH$, reagent grade) was supplied by VWR. Gases ($N_2$ (>99.99%), $CO_2$ (>99.99%), and $O_2$ (>99.99%)) used for gas and water vapor permeation were purchased from Messer France S.A.S. All reagents were used as received without further purification.

## 2.2 Synthesis of copolyesters

The copolyesters were synthesized according to Scheme 1. The preparation of ISC10C4 and IMC10C4 followed a previously published procedure.[12] ISC10PDD26, ISC10IPC, IMC10PDD26 and IMC10IPC were prepared according to the following steps: IS (or IM, 10 mmol), C10 (5 mmol) and PDD26 (or IPC, 5 mmol) were weighed in a 100 mL three-necked round-bottomed flask equipped with a mechanical stirrer and a condenser. With the introduction of a continuous $N_2$ flow, 15 mL of toluene was added and the flask was dipped into an oil bath (80 and 95 °C for IS and IM, respectively). When the solid particles (IS and PDD26) disappeared, 5 mL of pyridine was added dropwise and the temperature was kept at 80 °C (or 95 °C) for 12 h, then increased to 115 °C and maintained for 12 h under $N_2$ atmosphere. After cooling to room temperature, the media were precipitated in methanol and purified 3 times by repeated dissolution/precipitation ($CH_2Cl_2$/$CH_3OH$). Finally, they were dried for 2 days at 40 °C under reduced pressure (15 mbar).

## 2.3 Preparation of polymer films

The polymer films were prepared by compression molding using a hot press machine from Scamex (Press 20 ton 300 × 300). Film thickness was controlled to be around 150 μm using the thickness of an aluminum window. Each

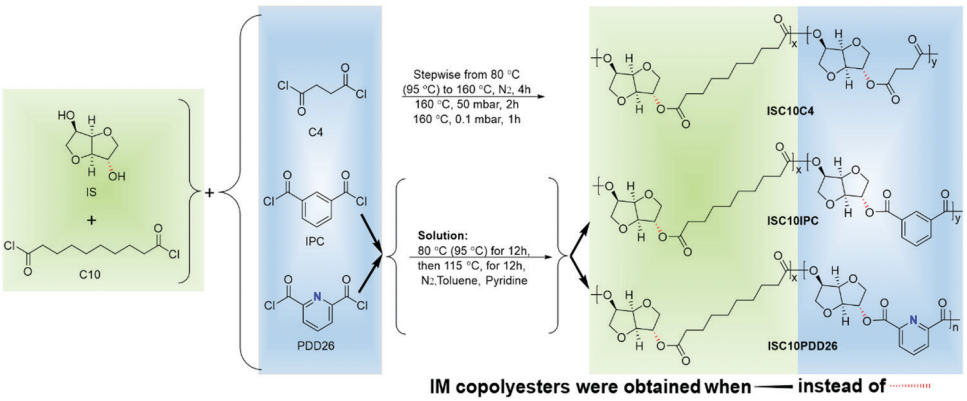


Scheme 1 Synthesis of IS and IM random copolyesters.

sample was pressed for 5 min under 50 bars according to the measured thermal properties (30–60 °C above $T_g$ or just above $T_m$) and then stored in a desiccator at room temperature under vacuum with $P_2O_5$ protection before measurements. IMC10C4 was isothermally crystallized at 55 °C for 3 days before storage. The fully transparent films obtained are shown in Fig. 1.

### 2.4 Size exclusion chromatography (SEC)

The copolyester molar masses were measured by size exclusion chromatography (PL-GPC50 from Varian) at 25 °C using two PLgel MIXED-C 5 μm (300 × 7.5 mm) columns and a RI detector. The samples were prepared by dissolving polymers (≅10 mg) in dichloromethane (1.7 mL, HLPC grade), and PMMA standards were used for calibration.

### 2.5 Fourier transform infrared (FTIR)

FTIR measurements were performed using a Spectrum Two instrument from PerkinElmer, in the ATR mode (diamond cell) at 25 °C. Each sample was scanned 10 times from 4000 to 650 $cm^{-1}$.

### 2.6 $^1$H nuclear magnetic resonance ($^1$H NMR)

Chemical structures were determined by $^1$H NMR (Bruker, 300 MHz) with a TopSpin acquisition system at room temperature (20 °C) in $CDCl_3$. The chemical shifts ($\delta$) were expressed in parts per million (ppm) and referenced to the non-deuterated residual solvent peak ($\delta$ = 7.26 ppm).

### 2.7 Thermogravimetric analysis (TGA)

The thermal stability of the polymers was investigated by TGA (Q500 from TA Instruments) under nitrogen atmosphere. Two aluminum layers were used to protect the platinum pan from corrosion by the potentially released chlorine. Around 10 mg of the sample was loaded in the pan and heated from 30 to 600 °C at a heating rate of 10 °C $min^{-1}$.

### 2.8 Differential scanning calorimetry (DSC)

The thermal properties of the polymers were investigated by DSC (Q2000 from TA Instruments). Around 10 mg of the sample was enclosed in an aluminum pan, and heated under a $N_2$ atmosphere from −30 to 200 °C at 10 °C $min^{-1}$, followed by cooling and a second heating.

### 2.9 Tensile tests

The mechanical properties of the polymer films were established by tensile tests at room temperature (23 °C) using a ZwickRoell Z010 apparatus with testXpert II software. A 500 N load cell and 10 mm $min^{-1}$ cross-head speed were operated. The dumbbell-shaped specimens were 1BB type according to ISO 527-2. More than 8 tests were performed on each sample to determine the final average value.

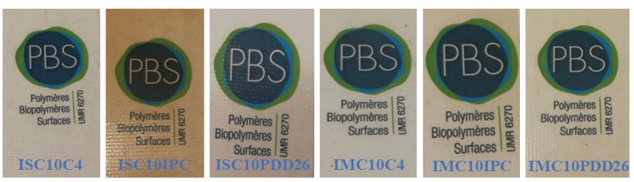


Fig. 1 Copolyester films prepared by hot pressing.

### 2.10 Surface energy

The water contact angle $\theta_w$ (°) and surface energy $\gamma^t$ (mN $m^{-1}$) with polar ($\gamma^p$) and dispersive ($\gamma^d$) parts were determined on films at room temperature (23 °C) with water (MilliQ Millipore® Water system), ethylene glycol, and decane. The size of the droplet was controlled to 3 μL and the photo time within 500 ms. Each result was averaged from at least five measurements. The surface energy was calculated using Windrop++ Carrousel software according to the Owens & Wendt method.

### 2.11 Liquid water sorption

The liquid water sorption measurements were performed at 25 °C. The measurement was performed in triplicate for each sample ($A$ = 1 $cm^2$) using a balance (precision 0.1 mg): the initially dry film ($m_d$) was immersed into pure water (MilliQ Millipore Water system) and the film mass ($m_t$) was periodically weighed by carefully removing the surface water. Then, the variation of the mass gain ($M_t$) *vs.* time ($t$) was calculated according to eqn (1).

$$M_t = \frac{m_t - m_d}{m_d} \times 100 \quad (1)$$

### 2.12 Water vapor sorption

The water vapor sorption behavior of the film was evaluated using the DVS1 Advantage apparatus (Surface Measurement Systems Ltd) at 25 °C as described before.[21] Different water vapor activity steps ($a_w$ = 0–0.95) were applied to the initially dry film ($m_d$ ≅ 15 mg). Each step was completed when an equilibrium ($m_{eq}$) was attained. The water vapor sorption isotherms were plotted according to the mass gain at equilibrium $M_{eq}$ (eqn (2)) *vs.* $a_w$.

$$M_{eq} = \frac{m_{eq} - m_d}{m_d} \times 100 \quad (2)$$

### 2.13 Water vapor permeation

The water vapor permeation measurements were performed at 25 °C using a previously described permeation cell.[22] The water vapor flux $J$ through the film ($A$ = 3.6 $cm^2$) as a function of time $t$ was measured at different $a_w$. The permeability coefficient $P$ was calculated at the steady-state ($J_{st}$) according to eqn (3), where $\Delta a_w$ is the difference in water activity across the film (thickness $L$).

$$P = \frac{J_{st} \times L}{\Delta a_w} \quad (3)$$

### 2.14 Gas permeation

The gas ($CO_2$, $O_2$ and $N_2$) permeation measurements were performed at 25 °C according to the previously described

time-lag method (upstream pressure $p_1$ = 4 bar and downstream compartment initially under vacuum).[23] The permeability coefficient $P$ (expressed in barrer, 1 barrer = $10^{-10}$ cm$^3$ (STP) cm cm$^{-2}$ s$^{-1}$ cmHg$^{-1}$) was calculated according to eqn (4):

$$P = \frac{L}{A\Delta P}\frac{\mathrm{d}Q}{\mathrm{d}t} \quad (4)$$

where $L$ is film thickness, $A$ is film surface area (11.34 cm$^2$), $\Delta P$ is the pressure difference between upstream and downstream compartments, $Q$ is the detected quantity of gas that crossed the film at time $t$ (s), and $\mathrm{d}Q/\mathrm{d}t$ is the slope of the experimental curve at the stationary state.

The gas diffusion coefficient $D$ was calculated according to eqn (5) ($t_L$ is the time-lag value obtained from the extrapolation of the steady-state asymptote to the time axis):

$$D = \frac{L^2}{6t_L} \quad (5)$$

# 3. Results and discussion

## 3.1 Molar masses

ISC10C4 ($\overline{M_n}$ = 18 000 g mol$^{-1}$) showed a higher molar mass than IMC10C4 ($\overline{M_n}$ = 13 000 g mol$^{-1}$). This was probably due to the decreased reactivity already observed in our previous work between IM and C4 which resulted in lower molar masses for IMC4. The copolymerization involving aromatic moieties was much more difficult to achieve in bulk since their rigidity reduced chain-end mobility.[24] Thus, the synthesis in toluene with pyridine (method established by Storbeck *et al.*[25]) was tried. The molar masses are presented in Table 1. The higher molar masses obtained with IS compared to IM were probably due to the higher reactivity of IS.[8] Unfortunately, a general decrease in molar masses was observed when incorporating aromatic moieties, such as IPC and PDD26. This confirmed the difficulty already encountered in producing high molar mass polyesters with 1,4:3,6-dianhydrohexitols and aromatic compounds.[8] However, satisfactory molar masses above 10 000 g mol$^{-1}$ were still obtained, with high yields around 90%.

## 3.2 Structures

The FTIR spectra (Fig. S1, ESI†) showed the C=O and C–O of ester groups stretching at 1730 and 1340–1130 cm$^{-1}$, respectively, which firstly confirmed the successful esterification. Then, the successful copolymerization was confirmed by the signals of the functional groups of the different components: $CH_2$ stretching at 3050–2820 cm$^{-1}$, aromatic C=C stretching at 1584 cm$^{-1}$, ester C–O stretching for aromatics at 1309, 1295, 1316, 1298 cm$^{-1}$, and for aliphatics at 1235, 1230, 1157, 1234, 1228 and 1154 cm$^{-1}$.

All proton signals found at the expected chemical shifts in $^1$H NMR spectra (Fig. S2, ESI†) further confirmed the chemical structures. The integrations globally corresponded to the different comonomers. The more split spectrum of ISC10C4 was due to the *exo–endo* stereoscopic effect of IS, which induced an irregular structure.[26] Besides, the more complex and split spectra of aromatic copolyesters compared to aliphatic ones were probably due to the structural difference between aliphatics and aromatics which induced distinct environments for hydrogens in IS and IM. The molar ratio of each component in the polymer was then calculated by considering the proton integrations of each comonomer (the equation is listed in Fig. S2, ESI†), shown in Table 1.

Table 1 General data obtained for the synthetic copolyesters

| Copolyester | ISC10C4 | ISC10IPC | ISC10PDD26 |
|---|---|---|---|
| $\overline{M_n}$[a] (g mol$^{-1}$) | 18 000 | 15 300 | 11 500 |
| $\overline{M_w}$[a] (g mol$^{-1}$) | 33 600 | 44 000 | 26 900 |
| $Đ$[b] | 1.9 | 2.9 | 2.3 |
| Yield[c] (%) | 91 | 90 | 85 |
| X : C10 : Y molar ratio in polymer[d] | 50 : 26 : 24 | 50 : 26 : 24 | 50 : 35 : 15 |
| $T_g$[e] (°C) | 30 | 61 | 40 |
| $T_m$[f] (°C) | — | — | — |
| $\Delta H_m$[f] (J g$^{-1}$) | — | — | — |

| Copolyester | IMC10C4 | IMC10IPC | IMC10PDD26 |
|---|---|---|---|
| $\overline{M_n}$[a] (g mol$^{-1}$) | 13 000 | 11 000 | 10 600 |
| $\overline{M_w}$[a] (g mol$^{-1}$) | 24 700 | 27 300 | 24 200 |
| $Đ$[b] | 1.9 | 2.5 | 2.3 |
| Yield[c] (%) | 89 | 89 | 86 |
| X : C10 : Y molar ratio in polymer[d] | 50 : 24 : 26 | 50 : 25 : 25 | 50 : 27 : 23 |
| $T_g$[e] (°C) | 30 | 55 | 64 |
| $T_m$[f] (°C) | 74/84/96[g] | — | — |
| $\Delta H_m$[f] (J g$^{-1}$) | 12 | — | — |

[a] SEC conducted in $CH_2Cl_2$ with PMMA standards. [b] Dispersity. [c] In precipitated polymer. [d] Calculated from $^1$H NMR; X is the diol (IS or IM); Y is the acyl dichloride. [e] DSC second heating. [f] DSC first heating. [g] Multiple peaks.

In general, the molar ratio of the polymer was almost the feeding molar ratio. The slight differences could be explained by the small-scale used for the synthesis: a small difference in monomer weighing cannot be ruled out, and controlling the accuracy of the feeding ratio to ensure the targeted stoichiometric ratio is a challenging factor. However, some bigger differences were observed when using PDD26, especially with IS, which may be linked to its lower reactivity.

## 3.3 Thermal degradation

Fig. 2 shows the thermal stability of copolyesters analyzed by TGA and the corresponding data are provided in Table S1 (ESI†). All copolyesters appeared to be thermally stable up to 328 °C with less than 5% weight loss. The copolyesters containing C4 and IPC showed higher thermal degradation temperatures compared to those containing PDD26, which could be linked with the higher C–C bond energy (83 kcal mol$^{-1}$) than the C–N bond energy (73 kcal mol$^{-1}$). No significant difference could be noticed between the use of IS and IM.

## 3.4 Differential scanning calorimetry (DSC)

The DSC thermograms of copolyesters are presented in Fig. 3 and the corresponding values are provided in Table 1.

As stated previously, the stereoscopic difference between IS and IM had little influence on $T_g$; nevertheless, some

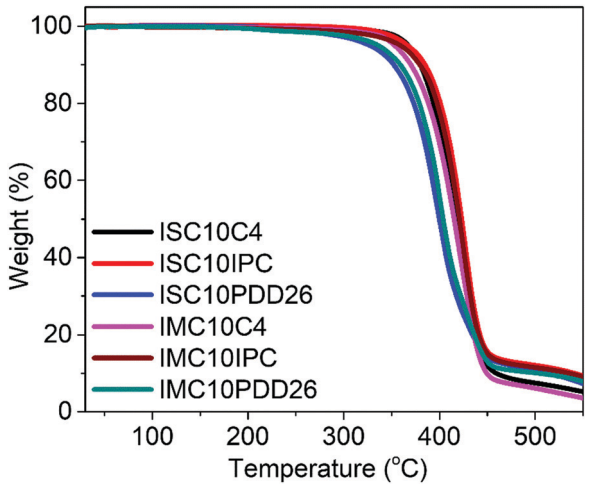


Fig. 2 TGA thermograms of copolyesters.

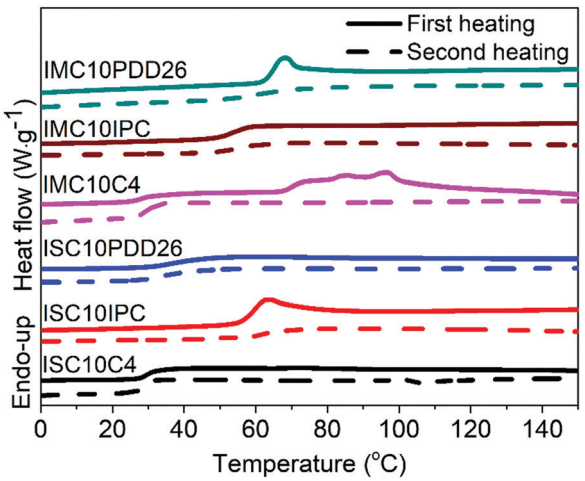


Fig. 3 DSC thermograms of copolyesters.

differences were observed between these copolyesters.[12,26] Considering ISC10IPC and IMC10IPC had the same molar composition in comonomers, the higher $T_g$ of ISC10IPC could be linked to its higher molar mass. On the contrary, ISC10PDD26 and IMC10PDD26 had similar molar masses, but IMC10PDD26 incorporated a much higher amount of PDD26, thus leading to a higher $T_g$. Finally, the same $T_g$ measured for ISC10C4 and IMC10C4 was a cooperation result of molar mass and monomer ratio. On the other hand, a higher $T_g$ was systematically obtained by incorporating aromatic moieties. Excluding ISC10PDD26 which had a low content of PDD26, the pyridine structure ($T_g$ = 64 °C for IMC10PDD26) was more efficient in improving $T_g$ than the benzene structure ($T_g$ = 55 °C for IMC10IPC). All copolyesters showed increased $T_g$ compared to ISC10 ($T_g$ = 2 °C) and IMC10 ($T_g$ = 0 °C).[12]

Unfortunately, the incorporation of comonomers prevented the polymers from crystallization, except IMC10C4 which exhibited a melting with $\Delta H_m$ = 12 J g$^{-1}$. Its multiple melting peaks ($T_m$ = 74/84/96 °C) with a wide melting range were probably due to a crystallization polymorphism coupling with a melting/crystallization/re-melting process, which is a common trait of linear polyesters comprising both semi-rigid and flexible chains.[14,26] However, the absence of melting during the DSC second heating indicated the difficulty encountered in reorganizing the molecular chain orderly from the melt.[27]

To provide preliminary information for IMC10C4 film preparation, the crystallization behavior of this polymer was further investigated by isothermal crystallization, after the first melting at 150 °C, at $T_i$ = 55 °C for 0 to 5 days ($t_i$) (Fig. S3, ESI†). After a broadening of the endothermic peak and an increase in the melting enthalpy when the crystallization time increased, the crystallization seemed to reach its final state after three days at 55 °C. Hence, these annealing conditions were used before IMC10C4 film preparation.

### 3.5 Mechanical properties

The representative tensile curves of polymer films are shown in Fig. 4 and the corresponding tensile parameters are recorded in Table 2.

Fig. 4 discloses the brittle fractures of semi-aromatic copolyesters and the plastic fractures of aliphatic ones. The incorporation of rigid comonomers, such as C4, IPC and PDD26, naturally increased the stiffness ($E$ increased at least 6 times) and the tensile strength ($\sigma_b$ increased at least 3 times) of ISC10 ($E$ = 127 ± 20 MPa, $\sigma_b$ = 4.2 ± 0.8 MPa, $\varepsilon_b$ = 19 ± 5%) and IMC10 ($E$ = 125 ± 10 MPa, $\sigma_b$ = 1.0 ± 0.2 MPa, $\varepsilon_b$ = 16 ± 3%), but decreased the elongation at break (except ISC10C4 which will be discussed later).[12] This phenomenon was even more observed for IPC and PDD26 (but to a lesser extent for ISC10PDD26 due to its lower PDD26 content) compared to C4: the aromatic moieties brought more chain stiffness, strength, and brittleness. Furthermore, despite a lower molar mass, IMC10C4 showed higher $E$ (1180 MPa) and $\sigma_b$ (21.0 MPa) and restricted elongation at break ($\varepsilon_b$ = 12%) compared to ISC10C4, certainly due to its crystallinity.

It should be stressed that ISC10C4 presented a very particular behavior. Indeed, the incorporation of C4 in ISC10C4 not

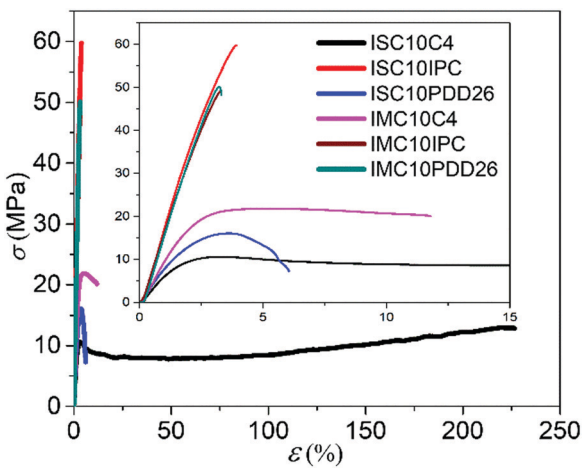


Fig. 4 The stress–strain curves of copolyester films.

Table 2 Tensile parameters of the copolyester films

| Polyester film | $E$ (MPa) | $\sigma_b$ (MPa) | $\varepsilon_b$ (%) |
|---|---|---|---|
| ISC10C4 | 770 ± 90 | 11.8 ± 1.1 | 220 ± 20 |
| ISC10IPC | 2100 ± 50 | 59.0 ± 1.7 | 3.6 ± 0.4 |
| ISC10PDD26 | 850 ± 80 | 8.0 ± 2.6 | 6.0 ± 1.5 |
| IMC10C4 | 1180 ± 80 | 21.0 ± 2.7 | 12.0 ± 1.0 |
| IMC10IPC | 1820 ± 30 | 50.0 ± 1.7 | 3.0 ± 0.3 |
| IMC10PDD26 | 1900 ± 40 | 50.0 ± 1.2 | 3.0 ± 0.4 |

$E$, Young's modulus; $\sigma_b$, stress at break; $\varepsilon_b$, strain at break.

only brought much higher $E$ (770 MPa *vs.* 127 MPa) and $\sigma_b$ (11.8 MPa *vs.* 4.2 MPa) compared to ISC10, but also largely increased $\varepsilon_b$ (220% *vs.* 19%).[12] The increase in $E$ and $\sigma_b$ was probably due to the increase of $T_g$, above room temperature, while the increase in $\varepsilon_b$ may be related to its high molar mass coupled with a $T_g$ close to the ambient temperature, thus even slight localized heating due to the tensile stress could favor chain disentanglement.[28] Another interesting phenomenon was observed for ISC10C4: the stretched sample, even after being broken at its maximum elongation (220%), recovered almost its original dimensions and retained only a 10% strain (5.5 cm *vs.* 5 cm) after being brought to the external temperature of the human body (35–37 °C) (Fig. S4 (ESI†) and attached video).

### 3.6 Contact angle

The copolyesters showed no obvious difference in surface properties (Table 3). Only a slightly lower $\theta_w$ (or higher $\gamma^t$) was observed for ISC10PDD26 and IMC10PDD26 compared to other copolyesters, probably due to the presence of the polar pyridine sites. All copolyesters showed similar surface energies and water contact angles compared to ISC10 ($\gamma^t$ = 31.0 mN m$^{-1}$, $\theta_w$ = 85 ± 1.0°) and IMC10 ($\gamma^t$ = 29.6 mN m$^{-1}$, $\theta_w$ = 83 ± 0.5°).[12]

### 3.7 Liquid water sorption

The liquid water sorption results are presented Fig. 5.

All copolyesters showed increased liquid water sorption compared to ISC10 ($M_{eq}$ = 0.55 ± 0.05%) and IMC10 ($M_{eq}$ = 1.03 ± 0.09%), which is probably because their large amorphous domain allows a larger water uptake.[29] ISC10PDD26 ($M_{eq}$ = 5.8 ± 0.5%) and IMC10PDD26 ($M_{eq}$ = 3.1 ± 0.3%) showed a higher liquid water sorption, which could be due to the presence of hydrophilic pyridine sites in the polymer structure. However, the higher water uptake of ISC10PDD26 compared to IMC10PDD26 was unexpected since ISC10PDD26 contained less pyridine moieties (30 mol% for ISC10PDD26; 45 mol% for IMC10PDD26). It should be mentioned that water sorption in polyesters is complex since water molecules show great interactions with the polymer matrix.[30] Thereby, the sorption of water molecules in polymers can lead to dimensional changes through the swelling of the polymer matrix and the decrease of the glass transition temperature ($T_g$), which will, in turn, result in larger water sorption.[30–32] Thus, the effect of liquid water sorption at $T_g$ for ISC10PDD26 and IMC10PDD26 was checked by DSC measurements (Fig. 6). $T_g$ after water sorption ($T_{g,H_2O}$) for ISC10PDD26 ($T_{g,H_2O}$ = 20 °C) was below the experimental temperature ($T$ = 25 °C), while for IMC10PDD26 ($T_{g,H_2O}$ = 43 °C) it remained above 25 °C. Even if $T_{g,H_2O}$ for both ISC10PDD26 and IMC10PDD26 was decreased by 20 °C, the high initial $T_g$ of IMC10PDD26 (64 °C) allowed its $T_{g,H_2O}$ to stay above 25 °C, in contrast to ISC10PDD26. The lower $T_{g,H_2O}$ of ISC10PDD26 than 25 °C indicated that the sample was in the rubber state with a larger free volume, which allowed higher water uptake.[33,34]

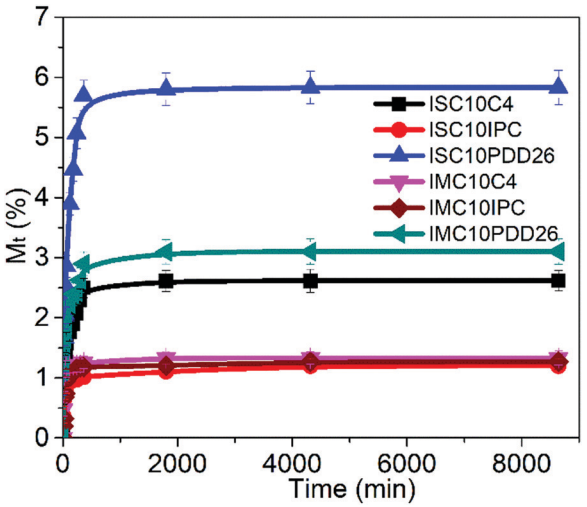


Fig. 5 Liquid water sorption of copolyester films.

More generally, we noticed that all the samples showed a decreased $T_g$ after water sorption, which is known as water-induced plasticization.[35,36] For ISC10IPC, IMC10IPC and IMC10PDD26, their high initial $T_g$ allowed preserving their glassy state because their final $T_{g,H_2O}$ stayed above 25 °C, in contrast to ISC10C4, ISC10PDD26 and IMC10C4. IMC10C4, IMC10IPC and ISC10IPC showed better resistance to water plasticization with a lower decrease of $T_g$. Consequently, the liquid water sorption was less pronounced for them. The nonpolar aromatic benzene ring in IPC and the semi-crystalline nature of IMC10C4 can explain this behavior. Combining the changes in $T_g$ with the water sorption behavior, we can generally conclude that the ability to resist water plasticization is an important factor determining the water sorption of these glassy state copolyesters.

Table 3 Surface energies and water contact angles of the copolyester films

| Polyester films | $\gamma^t$ (mN m$^{-1}$) | $\gamma^d$ (mN m$^{-1}$) | $\gamma^p$ (mN m$^{-1}$) | $\theta_w$ (°) |
|---|---|---|---|---|
| ISC10C4 | 28.8 | 23.4 | 5.4 | 86 ± 1.7 |
| ISC10IPC | 28.6 | 23.2 | 5.4 | 87 ± 1.2 |
| ISC10PDD26 | 30.5 | 24.2 | 6.3 | 84 ± 1.5 |
| IMC10C4 | 28.8 | 23.3 | 5.5 | 86 ± 0.8 |
| IMC10IPC | 28.3 | 23.1 | 5.2 | 87 ± 1.0 |
| IMC10PDD26 | 31.2 | 24.3 | 6.9 | 83 ± 1.3 |

$\gamma^t$, total surface energy with dispersive ($\gamma^d$) and polar ($\gamma^p$) parts; $\theta_w$, water contact angle.

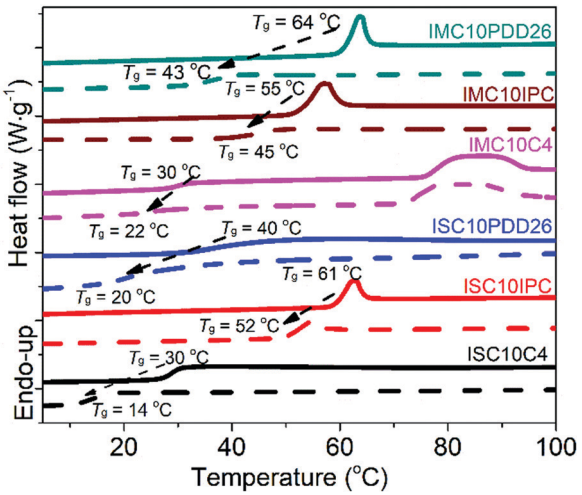


Fig. 6 The DSC thermograms of copolyester films before (solid) and after (dash) liquid water sorption.

### 3.8 Dynamic vapor sorption

The water vapor sorption isotherms of copolyester films are presented in Fig. 7.

All copolyesters exhibited an increase in water vapor sorption compared to ISC10 and IMC10 (*e.g.* $M_{eq}$ = 0.58% and $M_{eq}$ = 1.08% at water activity $a_w$ = 0.95, respectively).[12] The values at $a_w$ = 0.95 followed the same order as observed for liquid water sorption with the highest sorption value for ISC10PDD26 and the lowest for ISC10IPC. All isotherms displayed sigmoid profiles and obeyed the three steps of Park's model with a first Langmuir, then a Henry sorption and finally the aggregation of water molecules.[37] The corresponding Park's model parameters are provided in Table 4. At $a_w < 0.1$, typical Langmuir-type sorption is related to the adsorption of water molecules onto the specific hydrophilic sites, such as polar groups or micro-voids on the surface of films.[38] At this $a_w$, ISC10PDD26 and IMC10PDD26 exhibited higher sorption with larger $b_L$ values compared to other copolyesters due to their hydrophilic pyridine sites. The higher Langmuir constants of ISC10IPC compared to ISC10C4 are related to the Langmuir sites of the former ($A_L$ = 1.20 × $10^{-3}$ (g $g^{-1}$) *vs.* $A_L$ = 0.55 × $10^{-3}$ (g $g^{-1}$)). A possible explanation could be found in their structure: even though the whole benzene ring is a non-polar structure, the IPC ring has a dipolar moment greater than the C4 unit. The lowest Langmuir-type sorption of IMC10C4 was probably due to the presence of crystallites that reduced the value of $A_L$.[30,39,40] When the preferential sites were occupied, the isotherms became linear owing to random dissolution/diffusion (Henry's type sorption) of water molecules in the polymer matrix.[41] The solubility coefficient $S$ (analogous to $k_H$) can be then calculated from the slope of the linear part ($a_w$ = 0.2–0.7) of the isotherms. The large $S$ values for ISC10PDD26 ($S$ = 10.6 × $10^{-3}$ $g_{H_2O}$ $g_{pol}^{-1}$) and IMC10PDD26 ($S$ = 8.1 × $10^{-3}$ $g_{H_2O}$ $g_{pol}^{-1}$) could be explained by their hydrophilic pyridine sites. ISC10IPC ($S$ = 6.3 × $10^{-3}$ $g_{H_2O}$ $g_{pol}^{-1}$) and IMC10IPC ($S$ = 5.8 × $10^{-3}$ $g_{H_2O}$ $g_{pol}^{-1}$) showed lower solubility compared to ISC10C4 ($S$ = 8.3 × $10^{-3}$ $g_{H_2O}$ $g_{pol}^{-1}$) and IMC10C4 ($S$ = 7.1 × $10^{-3}$ $g_{H_2O}$ $g_{pol}^{-1}$), which was contrary to their Langmuir-type sorption. This was probably due to the larger water-induced polymer swelling of the latter,[30,32] which has been previously discussed for the liquid water sorption. At $a_w > 0.7$, an exponential increase of sorbed water concentration was observed due to the formation of water aggregates. $K_a$ values were larger for ISC10PDD26 and IMC10PDD26 indicating more water aggregates but with similar sizes regardless of the sample. This reveals that ISC10PDD26 and IMC10PDD26 were more hydrophilic than other copolyesters for the whole range of water vapor activity. It was not surprising that the polar pyridine sites showed strong affinities to water molecules.

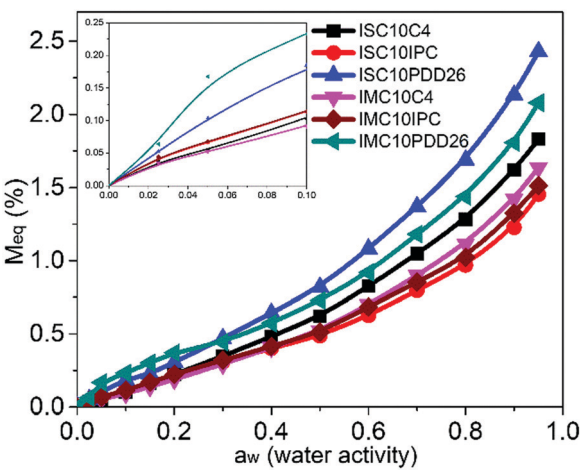


Fig. 7 The water vapor sorption isotherms of copolyester films.

### 3.9 Water vapor permeation

The water barrier properties were evaluated using water vapor permeation measurements as reported in Fig. 8.

The high $P_{H_2O}$ values over the entire water activity range for both ISC10C4 and ISC10PDD26 could be attributed to the polymer swelling. It is surprising to obtain a high $P_{H_2O}$ value for IMC10C4 because this polyester is semi-crystalline. This could be explained by its low $T_g$ that decreased in the presence of water and consequently induced large swelling at high $a_w$ values. The $P_{H_2O}$ values of ISC10IPC, IMC10IPC, and IMC10PDD26 were generally lowest and constant, which validated the ability of these polymers to resist swelling. The higher $P_{H_2O}$ values of IMC10PDD26 compared to those of ISC10IPC and IMC10IPC could be due to the higher water solubility brought by the polar pyridine sites. Then the lowest $P_{H_2O}$ values for ISC10IPC and IMC10IPC seemed reasonable, due to their resistance to swelling and low polarity. All copolyesters showed reduced $P_{H_2O}$ values compared to ISC10 and IMC10,[12] which was probably due to the increased $T_g$. Thus, we can generally conclude that the $T_g$ and polarity of these copolyesters were the two dominant factors that influence their water vapor permeation behaviors.

### 3.10 Gas permeation

As described in the experimental part, the gas permeation was conducted under differential pressure. However, IMC10IPC and

Table 4 Sorption parameters of the Park's model

| Polyester film | $A_L \times 10^3$ (g g$^{-1}$) | $b_L$ | $k_H \times 10^3$ (g g$^{-1}$) | $K_a \times 10^3$ (g g$^{-1}$) | $n_a$ |
|---|---|---|---|---|---|
| ISC10C4 | 0.55 ± 0.03 | 0.42 ± 0.01 | 10.6 ± 1.1 | 0.92 ± 0.05 | 4.0 ± 0.1 |
| ISC10IPC | 1.20 ± 0.07 | 0.47 ± 0.04 | 3.9 ± 0.2 | 0.85 ± 0.03 | 4.0 ± 0.2 |
| ISC10PDD26 | 0.55 ± 0.05 | 3.00 ± 0.20 | 15.5 ± 1.3 | 1.32 ± 0.13 | 3.0 ± 0.1 |
| IMC10C4 | 0.35 ± 0.02 | 0.40 ± 0.01 | 9.0 ± 0.5 | 0.87 ± 0.04 | 4.0 ± 0.1 |
| IMC10IPC | 1.30 ± 0.09 | 0.50 ± 0.03 | 3.7 ± 0.2 | 0.80 ± 0.03 | 5.0 ± 0.2 |
| IMC10PDD26 | 0.12 ± 0.01 | 38.4 ± 2.0 | 10.4 ± 0.9 | 1.00 ± 0.07 | 4.0 ± 0.1 |

$A_L$, Langmuir's capacity constant; $b_L$, Langmuir affinity constant; $k_H$, Henry's type solubility coefficient; $K_a$, equilibrium constant for clustering reaction; $n_a$, average number of water molecules per cluster.

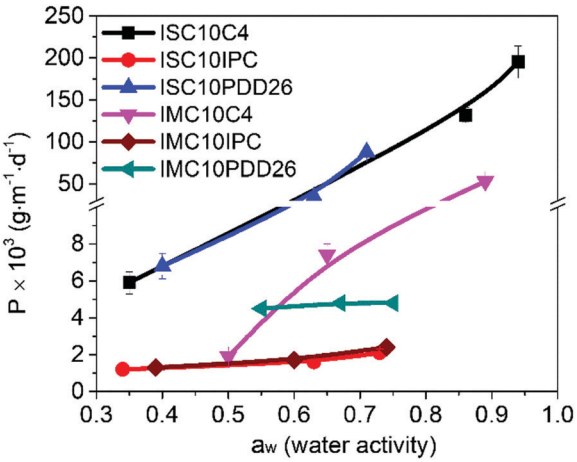


Fig. 8 Water vapor permeation coefficient ($P_{H_2O}$) of copolyester films at different water activities ($a_w$).

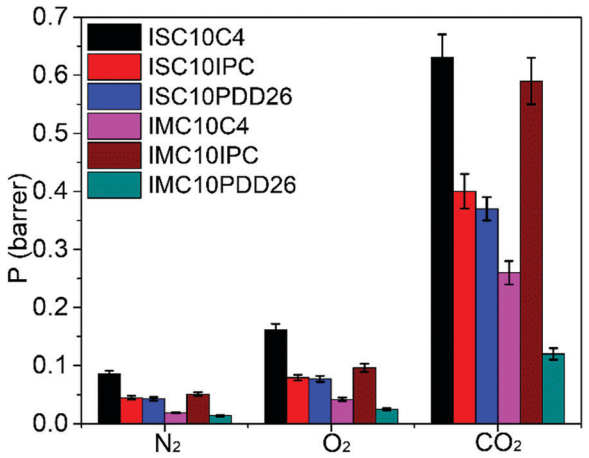


Fig. 9 Gas permeation coefficients ($P$) of copolyester films.

IMC10PDD26 were not resistant enough to the experimental pressure. Consequently, a PDMS membrane was used as a support to assist their gas permeation measurements. In this case, diffusion coefficient ($D$) values cannot be accurately calculated using the time-lag method, thus only permeation coefficients ($P$) were discussed for these two samples. Their $P$ values were calculated according to the law of resistors in series $\frac{P_t}{l_t} = \frac{P}{l} + \frac{P_{PDMS}}{l_{PDMS}}$, where $P_t$ and $l_t$ are the total permeability and thickness, $P_{PDMS}$ and $l_{PDMS}$ are the permeability and thickness of the PDMS membrane, and $P$ and $l$ are the permeability and thickness of the tested film. The gas permeation coefficients ($P$) for $N_2$, $O_2$ and $CO_2$ are presented in Fig. 9 (main data are provided in Table S2, ESI†).

Even with the loss of crystallinity, all copolyesters showed enhanced gas barrier properties (decreased $P$ values) compared to ISC10 ($P_{N_2}$ = 0.09 barrer, $P_{O_2}$ = 0.26 barrer, $P_{CO_2}$ = 1.32 barrer) and IMC10 ($P_{N_2}$ = 0.18 barrer, $P_{O_2}$ = 0.46 barrer, $P_{CO_2}$ = 2.04 barrer).[12] This was due to the increase in the $T_g$ values for all copolyesters: their glassy state at 25 °C (experimental temperature) allowed limited chain movements for gas penetration. All copolyesters showed $P$ values following the well-known order reported by Van Krevelen:[41] $P_{N_2} < P_{O_2} < P_{CO_2}$. This ranking is a result of the double dependence of permeability on diffusivity, mainly on the kinetic diameter of the permeants ($d_{N_2}$ (0.364 nm) > $d_{O_2}$ (0.346 nm) > $d_{CO_2}$ (0.33 nm)), and solubility, mainly on the critical temperature ($T_c$) of the permeants ($T_{c(CO_2)}$ (31 °C) > $T_{c(O_2)}$ (−118 °C) > $T_{c(N_2)}$ (−147 °C)).[34]

It is known that the large sorption of $CO_2$ molecules will plasticize a glassy polymer matrix.[42] However, $CO_2$ ($T_{c(CO_2)}$ = 31 °C) is much less condensable than water ($T_{c(H_2O)}$ = 374 °C); thus, the plasticization by $CO_2$ usually needs a high feeding pressure (depending on the polymer, but usually >10 bar).[43] Considering the low $CO_2$ feeding pressure (3 bar) in our case, the $CO_2$ plasticization effect will be ignored in our discussion.

It should always be kept in mind that $P$ is a combined result of $D$ (obtained by the time-lag method) and $S$ (deduced from $P$ and $D$ coefficients); any factor that affects $D$ and $S$ can consequently influence $P$. To support our discussion, the $S$ and $D$ values of ISC10C4, ISC10IPC, ISC10PDD26, and IMC10C4 are provided in Table 5.

Thus, the influence of several factors on the gas permeation properties was discussed. Firstly, the main chain type (aliphatic *vs.* aromatic) was investigated. The incorporation of aromatic moieties (ISC10IPC and ISC10PDD26) is generally more efficient in increasing gas barrier properties than the incorporation of the aliphatic one (ISC10C4). This was probably due to the higher chain stiffness which caused lower mobility of chain segments, thus creating diffusion restriction.[44] Concerning the

Table 5 Gas solubility and diffusion coefficients ($S$ and $D$) of IS copolyester films and IMC10C4 film

| | $D \times 10^{10}$ (cm$^2$ s$^{-1}$) | | | $S \times 10^3$ (cm$^3$(STP) cm$^{-3}$ cmHg$^{-1}$) | | |
|---|---|---|---|---|---|---|
| | $N_2$ | $O_2$ | $CO_2$ | $N_2$ | $O_2$ | $CO_2$ |
| ISC10C4 | 9.4 ± 0.6 | 16 ± 1 | 76 ± 5 | 9.0 ± 0.6 | 10.1 ± 0.6 | 8.3 ± 0.7 |
| ISC10IPC | 4.9 ± 0.3 | 8.2 ± 0.6 | 48 ± 3 | 9.2 ± 0.7 | 9.6 ± 0.6 | 8.3 ± 0.6 |
| ISC10PDD26 | 4.5 ± 0.3 | 6.8 ± 0.5 | 28 ± 2 | 9.5 ± 0.7 | 11.3 ± 0.8 | 13.3 ± 0.9 |
| IMC10C4 | 2.5 ± 0.2 | 5.4 ± 0.4 | 35 ± 2 | 7.7 ± 0.5 | 7.8 ± 0.6 | 7.4 ± 0.5 |

aromatic moieties (*m*-phenylene ring *vs.* 2,6-pyridine ring), the lower $P$ values of ISC10PDD26 and IMC10PDD26 compared to ISC10IPC and IMC10IPC indicated that the 2,6-pyridine ring structure brought more barrier properties. Considering that the copolyesters were amorphous, the lower gas permeability of ISC10PDD26 and IMC10PDD26 may be due to the polar pyridine ring which induced chain–chain (inter/intrachain) attractions, thus allowing a close chain–chain packing and restricting chain segmental motions.[45] Similarly, the higher PDD26 incorporation ratio could explain the higher gas barrier properties of IMC10PDD26 compared to ISC10PDD26. Besides, the semi-crystalline IMC10C4 was more barrier ($P_{N_2}$ = 0.019 barrer, $P_{O_2}$ = 0.04 barrer, $P_{CO_2}$ = 0.26 barrer) than amorphous ISC10C4 ($P_{N_2}$ = 0.084 barrer, $P_{O_2}$ = 0.12 barrer, $P_{CO_2}$ = 0.59 barrer), which was expected since crystallites are generally impermeable to gases.[46,47] This explanation was verified by both lower $S$ and $D$ values for IMC10C4. Finally, even if ISC10IPC showed slightly enhanced gas barrier properties than IMC10IPC, we cannot generally conclude that the *exo*/*endo* stereoscopic structure of IS was more barrier to gases than the *endo–endo* stereoscopic structure of IM, because the higher chain entanglement caused by the larger molar masses of ISC10IPC also decreases gas permeability.

To sum up, the enhanced $T_g$ effectively improved the gas barrier properties of ISC10 and IMC10 polyesters. Besides, retaining crystallinity is a supplemental positive factor for gas barrier properties. Regardless of the semi-crystalline nature of IMC10C4, the chemical structures of the introduced rigid moieties showed the abilities ($A_p$) to decrease $P$ values in the following order: $A_p$(PDD26) > $A_p$(IPC) > $A_p$(C4). All copolyesters showed better gas barrier than PLA containing 98% L-lactide ($P_{N_2}$ = 4.99 barrer, $P_{O_2}$ = 0.11–0.56 barrer and $P_{CO_2}$ = 1.88 barrer). Although the barrier properties of IMC10PDD26 were much lower than those of PEF ($P_{O_2}$ = 0.004 barrer and $P_{CO_2}$ = 0.012 barrer),[29] they were comparable to those of semi-crystalline PET ($P_{O_2}$ = 0.018–0.030 barrer and $P_{CO_2}$ = 0.12–0.16 barrer).[44] These efficient gas barrier properties of IMC10PDD26 may be attributed to its asymmetrical polar 2,6-pyridine ring.

## 4. Conclusions

This work was focused on the preparation of bio-based ISC10 and IMC10 copolyesters with enhanced properties. The general idea was to incorporate a third rigid monomer *via* copolycondensation. The third rigid monomer was either aliphatic (C4) or aromatic (IPC and PDD26). High molar masses were achieved for aliphatic copolyesters, while generally lower molar masses were obtained for aromatic ones. All copolyesters showed good thermal stability with $T_d^{5\%}$ higher than 328 °C and $T_g$ ranging from 30 to 64 °C. The third rigid monomer, and more generally the aromatic skeleton, especially the pyridine skeleton, significantly improved the $T_g$ of ISC10 and IMC10. All copolyesters showed improved barrier properties (both to water and gases) compared to ISC10 and IMC10. IMC10PDD26 showed the best gas barrier properties, which was linked to its pyridine structure. These high gas barrier properties were comparable to those of the widely used semi-crystalline PET.

## Conflicts of interest

There are no conflicts to declare.

## Acknowledgements

The authors thank the China Scholarship Council [grant number 201701810120] for financial support. They also thank Dr K. Fatyeyeva and Dr C. Chappey for permeation measurements.

## References

1 COP21-Paris Climate Conference 2015, https://www.gouvernement.fr/en/paris-climate-conference, accessed 2015-12-12.
2 The Paris Agreement, https://unfccc.int/process-and-meetings/the-paris-agreement/the-paris-agreement, accessed 2016-11-04.
3 Low-Carbon World, https://www.novabuild.fr/rendez-vous/low-carbon-world-23-24-juin-2021, accessed 2021-05-09.
4 Transition to low-carbon world needs to be faster, says DNV GL report – News – The Chemical Engineer, https://www.thechemicalengineer.com/news/transition-to-low-carbon-world-needs-to-be-faster-says-dnv-gl-report/, accessed 2020-09-17.
5 The companies leading the charge against food packaging waste, https://www.forbes.com/sites/katejacksonk/2021/03/27/the-companies-leading-the-charge-against-food-packaging-waste/?sh=5d3925565be1, accessed 2021-03-27.
6 S. Legrand, N. Jacquel, H. Amedro, R. Saint-Loup, M. Colella, J. P. Pascault, F. Fenouillot and A. Rousseau, *ACS Sustainable Chem. Eng.*, 2020, **8**, 15199–15208.
7 D. J. Saxon, A. M. Luke, H. Sajjad, W. B. Tolman and T. M. Reineke, *Prog. Polym. Sci.*, 2020, **101**, 101196.
8 F. Fenouillot, A. Rousseau, G. Colomines, R. Saint-Loup and J. P. Pascault, *Prog. Polym. Sci.*, 2010, **35**, 578–622.

9 POLYSORB®: a pure isosorbide from sorbitol, a starch derivative, https://www.roquette.com/industries/selected-products/industry-performance-materials-isosorbide, accessed 2021-05-10.
10 Polyester resin: plant-based POLYSORB® isosorbide for polyester resin, https://www.roquette.com/industries/performance-materials/polyesters, accessed 2021-05-13.
11 M. Okada, Y. Okada and K. Aoi, *J. Polym. Sci., Part A: Polym. Chem.*, 1995, **33**, 2813–2820.
12 X. L. Liu, N. Desilles and L. Lebrun, *Eur. Polym. J.*, 2020, **134**, 109846.
13 C. Lavilla and S. Muñoz-Guerra, *Green Chem.*, 2013, **15**, 144–151.
14 Q. F. Sousa, C. Vilela, A. C. Fonseca, M. Matos, C. S. R. Freire, G. J. M. Gruter, J. F. J. Coelho and A. J. D. Silvestre, *Polym. Chem.*, 2015, **6**, 5961–5983.
15 H. Y. Zhang, M. Jiang, Y. P. Wu, L. Li, Z. P. Wang, R. Wang and G. Y. Zhou, *ACS Sustainable Chem. Eng.*, 2021, **9**, 6799–6809.
16 S. V. Mankar, M. N. G. Gonzalez, N. Warlin, N. G. Valsange, N. Rehnberg, S. Lundmark, P. Jannasch and B. Z. Zhang, *ACS Sustainable Chem. Eng.*, 2019, **7**, 19090–19103.
17 M. K. McClintock, G. W. Fahnhorst, T. R. Hoye and K. Zhang, *Metab. Eng.*, 2018, **48**, 208–217.
18 A. Pellis, J. W. Comerford, S. Weinberger, G. M. Guebitz, J. H. Clark and T. J. Farmer, *Nat. Commun.*, 2019, **10**, 1–9.
19 S. K. Burgess, R. M. Kriegel and W. J. Koros, *Macromolecules*, 2015, **48**, 2184–2193.
20 S. K. Burgess, J. E. Leisen, B. Kraftschik, C. R. Mubarak, R. M. Kriegel and W. J. Koros, *Macromolecules*, 2014, **47**, 1383–1391.
21 N. Follain, S. Roualdes, S. Marais, J. Frugier, M. Reinholdt and J. Durand, *J. Phys. Chem. C*, 2012, **116**, 8510–8522.
22 S. Marais, M. Metayer and M. Labbe, *J. Appl. Polym. Sci.*, 1999, **74**, 3380–3395.
23 K. Fatyeyeva, A. Dahi, C. Chappey, D. Langevin, J. M. Valleton, F. Poncin-Epaillard and S. Marais, *RSC Adv.*, 2014, **4**, 31036–31046.
24 S. N. Vouyiouka, E. K. Karakatsani and C. D. Papaspyrides, *Prog. Polym. Sci.*, 2005, **30**, 10–37.
25 R. Storbeck, M. Rehahn and M. Ballauff, *Die Makromol. Chemie Macromol. Chem. Phys.*, 1993, **194**, 53–64.
26 H. Marubayashi, T. Ushio and S. Nojima, *Polym. Degrad. Stab.*, 2017, **146**, 174–183.
27 Q. Lu, Z. Yang, X. Li and S. Jin, *J. Appl. Polym. Sci.*, 2010, **116**, 2060–2070.
28 D. C. Prevorsek and B. T. De Bona, *J. Polym. Sci., Part B: Polym. Phys.*, 1981, **19**, 605–622.
29 S. K. Burgess, G. B. Wenz, R. M. Kriegel and W. J. Koros, *Polymer*, 2016, **98**, 305–310.
30 S. K. Burgess, D. S. Mikkilineni, D. B. Yu, D. J. Kim, C. R. Mubarak, R. M. Kriegel and W. J. Koros, *Polymer*, 2014, **55**, 6861–6869.
31 D. Langevin, J. Grenet and J. M. Saiter, *Eur. Polym. J.*, 1994, **30**, 339–345.
32 K. Galić and N. Ciković, *Polym. Test.*, 2001, **20**, 599–606.
33 B. Ben Doudou, E. Dargent, S. Marais, J. Grenet and Y. Hirata, *J. Polym. Sci., Part B: Polym. Phys.*, 2005, **43**, 2604–2616.
34 T. Messin, N. Follain, A. Guinault, G. Miquelard-Garnier, C. Sollogoub, N. Delpouve, V. Gaucher and S. Marais, *J. Membr. Sci.*, 2017, **525**, 135–145.
35 R. M. Hodge, T. J. Bastow, G. H. Edward, G. P. Simon and A. J. Hill, *Macromolecules*, 1996, **29**, 8137–8143.
36 C. L. Buquet, B. Ben Doudou, C. Chappey, E. Dargent and S. Marais, *J. Phys. Chem. B*, 2009, **113**, 3445–3452.
37 G. S. Park, *Synthetic Membranes: Science, Engineering and Applications*, Springer, Netherlands, Dordrecht, 1986, pp. 57–107.
38 J. Grank and G. S. Park, *Diffusion in Polymers*, CRC Press, London and New-York, 1996.
39 I. Erukhimovich and M. O. de la Cruz, *J. Polym. Sci., Part B: Polym. Phys.*, 2004, **45**, 3003–3009.
40 A. S. Michaels, W. R. Vieth and J. A. Barrie, *J. Appl. Phys.*, 1963, **34**, 1–12.
41 D. W. Van Krevelen and K. Te Nijenhuis, *Properties of polymers*, Elsevier, 4th edn, 2009.
42 R. Swaidan, B. Ghanem, E. Litwiller and I. Pinnau, *Macromolecules*, 2015, **48**, 6553–6561.
43 A. F. Ismail and W. Lorna, *Sep. Purif. Technol.*, 2002, **27**, 173–194.
44 G. L. Robertson, *Food packaging-principles and practice*, Taylor & Francis, 3rd edn, 2013.
45 L. Jia and J. Xu, *Polym. J.*, 1991, **23**, 417–425.
46 J. Trifol, D. Plackett, P. Szabo, A. E. Daugaard and M. Giacinti Baschetti, *ACS Omega*, 2020, **5**, 15362–15369.
47 H. Hu, R. Zhang, W. B. Ying, L. Shi, C. K. Yao, Z. Y. Kong, K. Wang, J. G. Wang and J. Zhu, *Polym. Chem.*, 2019, **10**, 1812–1822.